Development and Comprehensive Study of a Novel BNP Inhibitor for Corrosion Protection of D16T Aluminum Alloy in Model Formation Water

D. Asanova, R. Vardanyan, and N. Akatyev*
Faculty of Natural and Geographical Sciences,
M. Utemisov West Kazakhstan University,
Nazarbayev av. 162, Uralsk, Kazakhstan

doi: https://doi.org/10.15255/CABEQ.2025.2457

Original scientific paper
Received: November 4, 2025
Accepted: February 16, 2026

This study presents the development and evaluation of a novel ternary BNP corrosion inhibitor composed of boric acid (B-component), 1,4-phenylenediamine (N-component), and disodium hydrogen orthophosphate (P-component) for the protection of D16T aluminum alloy in model formation water. The inhibition performance was evaluated using gravimetric, electrochemical, and surface wettability techniques. The optimized BNP composition achieved a protection efficiency of 93.13 % at 31.2 mg dm^{-3} and significantly reduced the corrosion current density from $6.41 \cdot 10^{-6}$ to $2.16 \cdot 10^{-6}$ A cm^{-2}. The inhibitor decreased the apparent activation energy and increased surface hydrophobicity, indicating the formation of a protective surface layer. Inhibitor adsorption obeyed the Langmuir and Freundlich isotherms, indicating additional heterogeneous surface interactions, and was characterized as spontaneous and endothermic. Electrochemical results suggested mixed-type inhibition mechanism. The results indicate that cooperative interactions between the B-, N-, and P-components promoted the formation of a stable protective layer, highlighting the potential of multicomponent inhibitor systems for corrosion protection of aluminum alloys in aggressive oilfield environments.

Keywords
BNP inhibitor, corrosion, adsorption, aluminum, metal protection, formation water

Introduction

Corrosion control represents a major challenge in the oil and gas industry, as the simultaneous presence of water, acidic species, dissolved oxygen, and brines in pipelines creates a highly aggressive environment. The rate and severity of corrosion depend on the nature and concentration of corrosive agents, as well as operating parameters such as temperature, pressure, and flow regime[1].

In recent years, various approaches have been adopted to mitigate corrosion, including the development of advanced metallic alloys, use of protective coatings, replacement of metallic components with composite materials, and the application of highly efficient corrosion inhibitors[2]. Among these methods, corrosion inhibitors are one of the most widely implemented strategies, because they can be injected into operating systems without process shutdown, are comparatively cost-effective, and do not require highly specialized technical procedures[3].

Aluminum is the second most widely used engineering metal, and its consumption continues to increase steadily due to the rapid expansion of industrial applications[4]. Aluminum and its alloys are employed in industrial applications owing to their favorable strength-to-weight ratio, recyclability, and natural ability to form a passive oxide film that provides a degree of corrosion resistance[5]. Nevertheless, in weakly acidic, chloride-containing environments such as formation waters, this protective oxide layer is susceptible to localized breakdown, resulting in pitting and crevice corrosion[6]. These environments are of practical importance in oilfield operations, heat exchangers, pipelines, and storage systems, where aluminum alloys frequently come into contact with brines and process solutions containing chloride ions and organic acids. The resulting degradation not only compromises structural integrity but also shortens service life, leading to increased maintenance and replacement costs. This has created a pressing need for the development of effective corrosion inhibitors capable of stabilizing the aluminum surface in such aggressive media.

The selection of an appropriate corrosion inhibitor for aluminum in aggressive oil and gas production environments requires a comprehensive assessment that integrates inhibition efficiency, environmental compliance, operational compatibility, and economic viability. Although aluminum is widely used owing

*E-mail: n.akatyev.science@gmail.com

to its low density and favorable mechanical properties, its long-term performance critically depends on the application of carefully tailored corrosion protection strategies to ensure the integrity and reliability of industrial equipment under service conditions[7].

In the oil and gas industry, formation water (FW) is the naturally occurring water found within hydrocarbon-bearing reservoirs[8] or any water that has been injected into the reservoir to enhance oil recovery[9]. The chemical composition of FW is complex and can vary significantly depending on the geographic location, the geological formation, the depth of the reservoir, and the age of the well[10]. FW is typically a brine with sodium and chloride as the dominant ions[11]. This salinity makes it highly corrosive and unsuitable for release into the environment without treatment[12]. Therefore, the development of effective corrosion inhibitors for metals in formation water represents an urgent and practically important research challenge.

Corrosion inhibitors employed in the oil and gas industry are often present as multicomponent systems. An important requirement for such formulations is that the individual components act in a cooperative manner. When synergistic interactions are established among the components, the total inhibition efficiency is enhanced, allowing effective corrosion protection to be achieved at lower inhibitor concentrations[13]. Therefore, modern research trends are heavily focused on finding synergistic combinations where the combined effect is greater than the sum of the parts. This includes combining different types of organic inhibitors or organic inhibitors with inorganic compounds[14]. Such mixed systems are often classified as mixed-type inhibitors because they inhibit both the anodic (oxidation) and cathodic (reduction) corrosion processes[15] and offer several advantages in corrosion protection. They enhance total efficiency by simultaneously reducing metal dissolution and hydrogen evolution, often benefiting from synergistic effects when combining different functional groups or compounds[16]. Additionally, mixed inhibitors are versatile across varying environmental conditions, they form protective films to shield metals from aggressive media, and, in many cases, are environmentally friendly[17,18]. For instance, a wide range of combined corrosion and scale inhibitors has been developed with specific properties for various field requirements, validated by laboratory experiments and industrial field application feedback[19]. Moreover, the BNP system containing boric acid, 1,4-phenylenediamine and trisodium orthophosphate at 3:2:1 molar ratio has demonstrated a high inhibition efficiency for carbon steel in 0.5 mol dm^{-3} hydrochloric acid solution, as previously reported[20].

The primary objective of this work was to expand the application scope of such multicomponent inhibitors and to develop an effective mixed-type inhibitory system for aluminum.

Materials and methods

Corrosion media and inhibitor preparation

All analytical-grade reagents were purchased from Sigma Aldrich, Merck, and Alfa Aesar, and used without any further purification. The corrosion medium (model FW[21]) consisting of 0.25 g dm^{-3} CH_3COOH + 5.0 g dm^{-3} NaCl (pH = 2.92 ± 0.08) was prepared by dissolution of the required amount of glacial acetic acid and sodium chloride in double-distilled water (DDW).

This mixture is a low-complexity FW that reproduces two key corrosivity factors found in many oilfields and produced waters, in particular, chloride ions (ionic strength, pitting risk) and a small concentration of organic acid (acetic acid) that lowers pH and simulates weak organic acids present in reservoir fluids. The investigated BNP compositions were prepared by dissolving the reagents directly in the corrosion medium. All mass measurements were performed using an Ohaus Adventurer Pro AV264 analytical balance with an accuracy of ±0.1 mg.

Specimen preparation

D16T aluminum alloy specimens with the following composition (wt.%): 92.7 % – Al; Cu – 4.6 %; Mg – 1.6 %; Mn – 0.6 %; Fe –0.19 %; Si – 0.17 %; Zn –0.07 %; and dimensions of 25.0 x 30.0 x 3.0 mm were obtained from an industrial supplier and used for corrosion testing. Prior to testing, the specimens were sequentially polished using emery papers with grit sizes ranging from 250 to 1200. They were then immersed in an alkaline solution (40 g dm^{-3} of NaOH in water) for 10 s, thoroughly rinsed with DDW, rapidly dried with an air stream, and stored in a desiccator to prevent exposure to the external environment until use.

Weight loss (gravimetric) assay

Weight loss experiments were conducted to determine the corrosion rate (CR), inhibition efficiency (IE), and surface coverage (θ). After pretreating, the metal specimens were immersed for 10 s in an alkaline solution (40 g dm^{-3} of NaOH in water) to remove the surface oxide layer. The samples were then rapidly rinsed with DDW and immediately transferred into 150 mL beakers containing 100 mL of the corrosion medium, with or without the inhibitor.

After the immersion period, the specimens were removed from the beaker and cleaned from corrosion products by immersing in a 1:1 nitric acid solution for 5 min at ambient temperature[22]. The coupons were thoroughly rinsed with DDW, washed sequentially with ethanol and acetone, dried, and re-weighed.

The corrosion rate (CR/mg m^{-2} h^{-1}), inhibition efficiency (IE$_{wl}$/%), and surface coverage (θ) were calculated according to Eqs. 1–3 respectively[23]:

$$\mathrm{CR\ (mg\ m^{-2}\ h^{-1})} = \frac{\Delta m}{S \cdot \tau} \tag{1}$$

$$\mathrm{IE_{wl}\ (\%)} = \frac{\mathrm{CR_0 - CR_i}}{\mathrm{CR_0}} \cdot 100 \tag{2}$$

$$\theta = \frac{\mathrm{IE_{wl}}}{100} \tag{3}$$

where Δm is the weight loss of D16T aluminum alloy coupon (mg) after the period of immersion (τ, h), S is the specimen surface area (m^2), CR$_0$ is the corrosion rate of D16T aluminum alloy without inhibitor, CR$_i$ is the corrosion rate of D16T aluminum alloy in the presence of inhibitor.

Electrochemical measurements

Electrochemical measurements were performed using a PGSTAT 101 potentiostat/galvanostat (Metrohm), controlled by NOVA 2.1.8 software with a three-electrode cell configuration: Ag/AgCl (3 M KCl) as the reference electrode (RE), platinum as the counter electrode (CE), and a D16T aluminum alloy coupon as the working electrode (WE). Measurements were conducted in model FW in the absence and presence of the BNP inhibitor at various concentrations.

The electrochemical cell for potentiodynamic measurements consisted of 100 mL of model FW in the absence and presence of varying concentrations of BNP inhibitor in a 150 mL glass beaker at room temperature. The WE, with an exposed area of 1.00 cm^2 was stabilized at open-circuit potential (OCP) testing at 1800 s.

The linear polarization measurements were performed immediately after OCP by running a linear sweep voltammetry (LSV) scan and corrosion rate analysis. The potentiodynamic scan was performed from –0.50 to +0.50 V at a scan rate of 0.001 V s^{-1} with a step voltage of 0.001 V. Corrosion potential (E_{corr}) and corrosion current density (j_{corr}) were determined from the Tafel polarization curves.

Inhibition efficiency (IE$_j$/%) based on corrosion current density[24] was calculated using Equation 4:

$$\mathrm{IE_j(\%)} = \frac{j_{corr} - j_{inh}}{j_{corr}} \cdot 100 \tag{4}$$

where j_{inh} and j_{corr} are the corrosion current densities determined by extrapolating the Tafel slopes with and without inhibitor, respectively, in A cm^{-2}.

From the values of the polarization resistance with and without inhibitor, the inhibition efficiency (IE$_R$/%) was calculated using Equation (5)[25]:

$$\mathrm{IE_R\ (\%)} = \frac{R_p^{inh} - R_p^0}{R_p^{inh}} \cdot 100 \tag{5}$$

where R_p^{inh} and R_p^0 represent the polarization resistance in the presence and absence of the BNP-inhibitor, respectively, Ω.

Chronopotentiometric (CP) (E *vs.* t) measurements for the D16T aluminum alloy samples were performed immediately after immersion in model FW containing the maximum concentration of BNP inhibitor (31.2 mg dm^{-3}) for 2 h. Polarization measurements were performed after 0, 0.5, 1, 1.5, and 2 h of immersion.

Chronoamperometry (CA) was used to evaluate protective film stability. For this purpose, 50.0 mV anodic or cathodic overpotentials (E_{corr} ± 50.0 mV) were applied to the system for 1800 s, and current density was plotted against operation time. The same measurements were performed in blank solution for comparison.

Contact angle measurements

Contact angle measurements are used in corrosion inhibitor studies to evaluate the wettability of a metal surface and the effectiveness of an inhibitor in altering the surface's properties. Contact angle measurements help determine whether the surface becomes hydrophobic after immersion in a solution containing a corrosion inhibitor. A higher contact angle indicates increased hydrophobicity[26], which reduces the interaction between the corrosive medium and the metal surface, thereby enhancing corrosion resistance. The wettability properties of the alloy surfaces were evaluated by measuring the contact angle formed between a DDW water droplet and the alloy surface using an Ossila contact angle goniometer with Ossila Contact Angle Software version 4.2.0. Water droplets (0.052 ± 0.005 mL) were carefully dispensed onto the sample surface using a microsyringe equipped with a 0.4 mm diameter needle. Contact angle values represent the average of at least three independent measurements taken at different locations on each sample. High-resolution images of the droplets were captured using a video camera system coupled with the analysis software. The contact angle was measured immediately after the metal specimens were re-weighed following exposure to a corrosive medium in the presence and absence of the BNP inhibitor.

Table 1 – *Corrosion rate (CR, mg m^{-2} h^{-1}), inhibition efficiency (IE_{wl}, %), and surface coverage (θ) of BNP compositions based on H_3BO_3, 1,4-PDA, and Na_3PO_4 against corrosion of D16T aluminum alloy in model FW as a function of components ratio after 18 h immersion*

Entry	Component concentration, $x \cdot 10^{-4}$ mol dm^{-3}			CR, mg m^{-2} h^{-1}	IE_{wl}, %	θ
	H_3BO_3	1,4-PDA	Na_3PO_4			
1	–	–	–	45.1	–	–
2	1	1	1	11.0	75.61	0.7561
3	1	3	1	13.0	71.18	0.7118
4	1	1	3	14.3	68.29	0.6829
5	1	3	3	19.6	56.54	0.5654
6	3	3	3	19.0	57.87	0.5787
7	1	2	2	40.0	11.31	0.1131
8	1	2	3	16.1	64.30	0.6430
9	3	1	3	25.8	42.79	0.4279
10	3	2	1	20.2	55.21	0.5521

Results and discussion

Development of optimal inhibitor composition by weight loss measurement

The investigation began with screening the corrosion inhibition performance of three-component mixtures based on boric acid, 1,4-phenylenediamine (1,4-PDA), and Na_3PO_4 at different molar ratios in the model FW. The experiments were conducted at concentrations ranging from 1 to $3 \cdot 10^{-4}$ mol dm^{-3} for each component, and the results are summarized in Table 1.

As shown in Table 1, the highest inhibition efficiency was obtained for the BNP composition based on H_3BO_3, 1,4-PDA, and Na_3PO_4 at a concentration of $1 \cdot 10^{-4}$ mol dm^{-3} with an equimolar ratio of 1:1:1, reaching 75.61 % (Entry 2). All other investigated molar ratios resulted in noticeably lower protection efficiencies, which did not exceed 72 % (Entries 3–10). These results demonstrate that an optimal proportion of the individual components was required to achieve high corrosion inhibition performance.

Table 2 – *Corrosion rate (CR, mg m^{-2} h^{-1}), inhibition efficiency (IE_{wl}, %), and surface coverage (θ) of BNP compositions against corrosion of D16T aluminum alloy in model FW as a function of component type at $1 \cdot 10^{-4}$ mol dm^{-3} for each component after 18 h immersion*

Entry	B – component	N – component	P – component	CR, mg m^{-2} h^{-1}	IE_{wl}, %	θ
1	–	–	–	45.1	–	–
2*	H_3BO_3	1,4-PDA	Na_3PO_4	11.0	75.61	0.7561
3	H_3BO_3	1,3-PDA	Na_3PO_4	16.0	64.52	0.6452
4	H_3BO_3	1,2-PDA	Na_3PO_4	36.7	18.63	0.1863
5	H_3BO_3	1,1'-biphenyl-4,4'-diamine (benzidine)	Na_3PO_4	51.5	N/R	N/R
6	H_3BO_3	1,4-PDA	Na_2HPO_4	3.1	93.13	0.9313
7	H_3BO_3	1,4-PDA	NaH_2PO_4	22.5	50.11	0.5011
8	H_3BO_3	1,4-PDA	K_3PO_4	27.3	39.47	0.3947
9	H_3BO_3	1,4-PDA	K_2HPO_4	13.2	70.73	0.7073
10	H_3BO_3	1,4-PDA	KH_2PO_4	31.6	29.93	0.2993
11	$Na_2B_4O_7$	1,4-PDA	Na_3PO_4	20.4	54.77	0.5477
12	H_3BO_3	1,4-PDA	$Na_4P_2O_7$	47.7	N/R	N/R
13	H_3BO_3	1,4-PDA	$K_4P_2O_7$	25.3	43.90	0.4390
14	H_3BO_3	1,4-PDA · 2HCl	Na_3PO_4	19.2	57.43	0.5743
15	H_3BO_3	$PhNH_2 \cdot HCl$	Na_3PO_4	42.3	6.21	0.0621
16	$C_6H_5B(OH)_2$	1,4-PDA	Na_3PO_4	22.5	50.11	0.5011

*data from Table 1 Entry 2

N/R – negative result

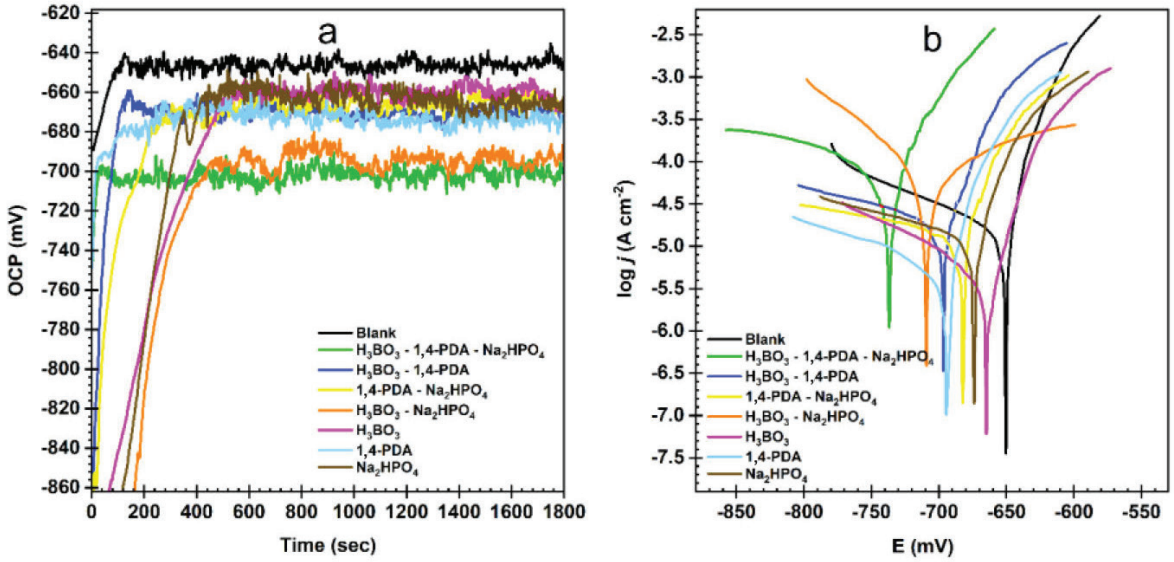

Fig. 1 – *Open-circuit potential (OCP) (a) and Tafel polarization curves (b) of mono-, di- and ternary-component systems containing H_3BO_3, 1,4-PDA, and Na_2HPO_4 ($1 \cdot 10^{-4}$ mol dm^{-3}) for D16T aluminum alloy in model FW at room temperature*

Based on these findings, and to enhance the protective efficiency of the inhibitor, the system was modified by successively replacing individual components with structurally related compounds from the same chemical classes while maintaining the same component ratio. The results are presented in Table 2.

The data presented in Table 2 demonstrate that replacing trisodium orthophosphate with the corresponding disodium salt led to a substantial enhancement in inhibitory efficiency, achieving 93.13 % (Entry 6). Conversely, substituting for other components, while maintaining the 1:1:1 molar ratio, did not lead to an improvement in protection performance.

To confirm the performance of the developed inhibitor more reliably, the system was further characterized using gravimetric measurements and electrochemical methods. For comparison, the individual components and their binary combinations were also examined. The open-circuit potential, Tafel polarization curves of the mono-, binary-, and ternary-component systems containing H_3BO_3–1,4-PDA–Na_2HPO_4 ($1 \cdot 10^{-4}$ mol dm^{-3}) for the protection of D16T aluminum alloy in model FW are presented in Fig. 1.

Table 3 presents the corresponding gravimetric and electrochemical parameters of the BNP compositions containing H_3BO_3, 1,4-PDA, and Na_2HPO_4 ($1 \cdot 10^{-4}$ mol dm^{-3}) for the protection of D16T aluminum alloy in model FW.

The obtained OCP profiles (Fig. 1a) reveal that the addition of inhibitor components led to a

Table 3 – *Gravimetric and electrochemical parameters of BNP compositions against corrosion of D16T aluminum alloy in model FW*

Entry	Component concentrations, $x \cdot 10^{-4}$ mol dm^{-3}			Weight loss assay			Polarization measurements			
	H_3BO_3	1,4-PDA	Na_2HPO_4	CR, mg m^{-2} h^{-1}	IE_{wl}, %	θ	OCP, mV	E_{corr}, mV	R_p, Ω	IE_R, %
1	–	–	–	45.1	–	–	–643.87	–658.68	1975.3	–
2*	1	1	1	3.1	93.13	0.9313	–702.97	–733.90	6721.2	70.61
3	1	1	–	30.9	31.55	0.3155	–671.44	–696.36	3243.1	39.09
4	–	1	1	26.8	40.65	0.4065	–668.74	–681.09	2567.2	23.06
5	1	–	1	28.9	35.90	0.3590	–687.36	–706.03	6347.4	68.88
6	1	–	–	51.7	N/R	–	–655.16	–663.12	2408.1	17.97
7	–	1	–	35.3	21.84	0.2184	–673.36	–693.55	3479.4	43.23
8	–	–	1	32.2	28.53	0.2853	–660.43	–673.82	2681.3	26.33

*data from Table 2

noticeable shift of the steady-state potential toward more negative values compared to the blank solution. Such shifts are frequently observed for aluminum systems and are often attributed to modifications in the stability and composition of the surface oxide/hydroxide layer and/or changes in the kinetics of cathodic reactions occurring on the alloy surface[27]. The ternary composition containing H_3BO_3, 1,4-PDA, and Na_2HPO_4 produced the largest potential shift, reaching approximately −703 mV, which indicates a substantial alteration of the metal/electrolyte interfacial processes. It is worth noting that the binary H_3BO_3–Na_2HPO_4 system also induced a comparable OCP shift, suggesting that these components play a dominant role in the inhibition mechanism.

The polarization curves (Fig. 1b) demonstrate a pronounced decrease in corrosion current density in the presence of inhibitor compositions. The ternary BNP composition provided the lowest corrosion rate (3.1 mg m^{-2} h^{-1}) and the highest inhibition efficiency according to gravimetric measurements (93.13 %). Consistently, electrochemical data show a substantial reduction in corrosion current and a significant increase in polarization resistance (6721.2 Ω), confirming its high protective performance.

From a mechanistic perspective, the enhanced performance of the ternary and H_3BO_3 – Na_2HPO_4 systems may tentatively be associated with cooperative interfacial effects. Boric acid is often reported to contribute to stabilization of hydrated oxide layers on aluminum surfaces[28], while orthophosphate species are known to participate in the formation of protective phosphate-containing surface films or to promote repassivation processes[29]. The combination of these species may therefore facilitate the development of a more compact and chemically stable surface barrier. The presence of 1,4-PDA may further modify adsorption characteristics and interfacial structure, potentially improving film integrity or surface coverage. Anodizing processes that include boric acid often result in films with improved corrosion resistance for this reason[30].

The reduction in corrosion current density observed for all inhibitor-containing solutions is a primary indicator of effective inhibition[31] and suggests that BNP compositions primarily suppress anodic metal dissolution while also influencing cathodic reactions[32]. The absence of substantial shifts in corrosion potential between different inhibited systems indicates that these inhibitors likely act through a mixed-type mechanism with a predominant surface-blocking effect suppressing both the anodic and cathodic reactions[33].

The high inhibition efficiency of the ternary mixture suggests the presence of synergistic interactions between components. The comparable performance of the H_3BO_3 – Na_2HPO_4 binary system indicates that these two constituents played a key role in establishing the protective interfacial layer, while 1,4-PDA appeared to enhance but not solely determine the total inhibition efficiency.

In summary, the obtained results demonstrate that BNP inhibitor provided substantial corrosion protection for D16T aluminum alloy in model FW. The experimental data suggest that the inhibition performance was governed by the cooperative action of all three components, with H_3BO_3 and Na_2HPO_4 species contributing significantly to protective layer formation.

In a further study, the composition of the developed BNP inhibitor was expressed in mg dm^{-3} in accordance with the weights of the components, as listed in Table 4.

At the next step of our study, the weight loss assay was applied to evaluate the inhibition efficiency of the developed three-component BNP inhibitor at various concentrations in model FW. The results are given in Fig. 2.

Fig. 2a demonstrates that, the presence of the BNP inhibitor significantly reduced the corrosion rate, and the extent of reduction increased with inhibitor concentration. At the highest concentration (31.2 mg dm^{-3}), the CR decreased during the first few hours and stabilized at a low value after approximately 10 h, suggesting the formation of a protective film on the metal surface[34].

Fig. 2b shows the corresponding inhibition efficiencies. The IE increased markedly with both concentration and immersion time, reaching more than 93.13 % at 31.2 mg dm^{-3} after 24 h. The initial increase in IE % reflects gradual adsorption of the inhibitor components onto the D16T alloy surface, while the subsequent stabilization indicates equilibrium between adsorption and desorption processes. These results confirm that the BNP inhibitor acted through adsorption-controlled surface protection, with efficiency strongly dependent on concentration and exposure time, leading to the formation of a stable, adherent film that effectively suppressed metal dissolution[35].

Effect of temperature and concentration

Fig. 3 illustrates the effect of inhibitor concentration and temperature on the corrosion rate (CR) and inhibition efficiency (IE) of the BNP compositions for D16T aluminum alloy in model FW after 2 h of immersion. The total concentration of the inhibitor is expressed in mg dm^{-3} in accordance with Table 4.

As shown in Fig. 3a, the corrosion rate decreased with increasing inhibitor concentration at all investigated temperatures (298–313 K), indicat-

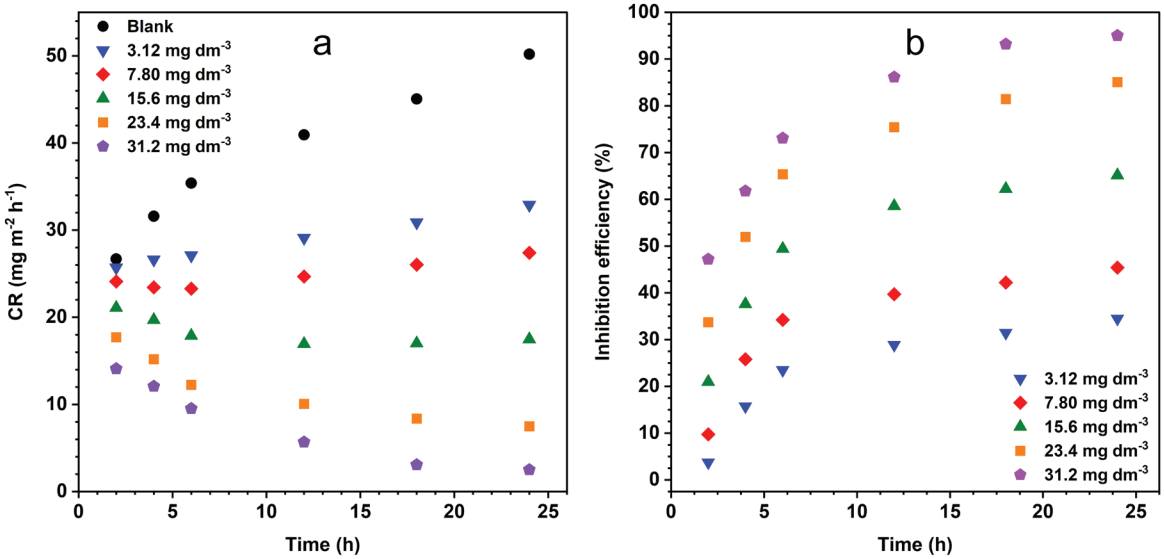

Fig. 2 – *Relationship between the CR (a) and inhibition efficiency (IE_{wl}) (b) for developed BNP inhibitor containing H_3BO_3-1,4-PDA-Na_2HPO_4 against corrosion of D16T aluminum alloy in model FW at varying inhibitor concentrations and immersion time at room temperature*

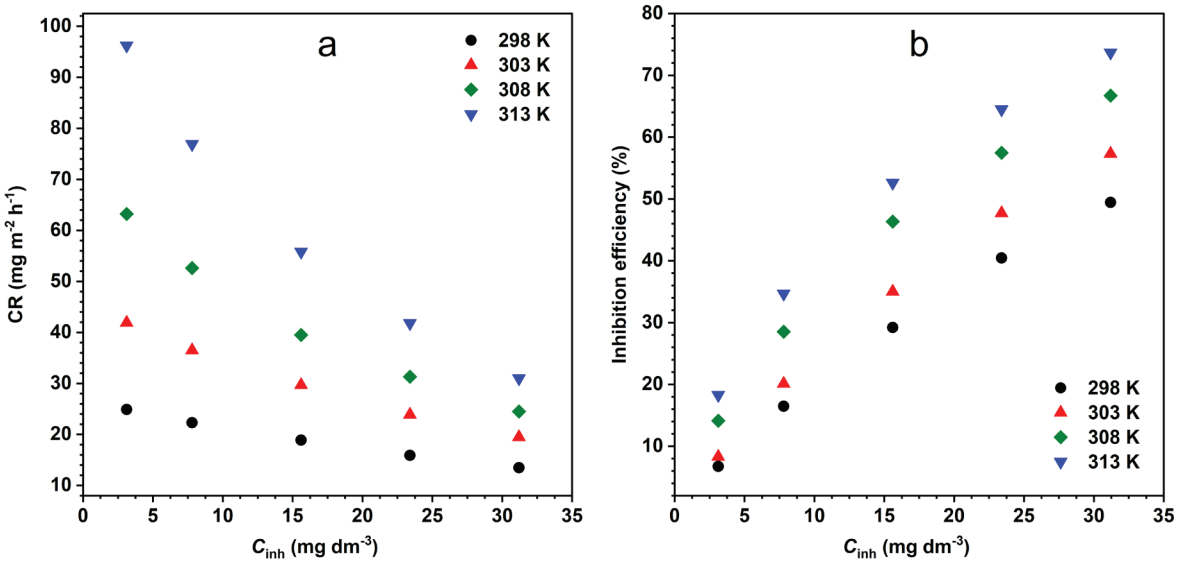

Fig. 3 – *Relationship between corrosion rate (CR) (a) and inhibition efficiency (IE) (b) for BNP inhibitor on D16T aluminum alloy in model FW in the absence and presence of different inhibitor concentrations after 2 h of immersion at different temperature*

ing progressive surface coverage by the inhibitor species. At a given concentration, the CR increased with temperature, reflecting the thermally activated nature of the corrosion process and the enhanced kinetics of metal dissolution in the blank and inhibited solutions. Nevertheless, even at 313 K, the presence of BNP significantly suppressed the corrosion rate compared to the uninhibited system, demonstrating the persistence of the protective effect over the studied temperature range.

The corresponding inhibition efficiencies (Fig. 3b) increased with inhibitor concentration and temperature, reaching maximum values at 31.2 mg dm^{-3}

Table 4 – *Total BNP inhibitor composition at varying concentrations and 1:1:1 component ratio*

H_3BO_3	1,4-PDA	Na_2HPO_4	Total BNP inhibitor concentration, mg dm^{-3}
$x \cdot 10^{-4}$ mol dm^{-3}			
0.1	0.1	0.1	3.12
0.25	0.25	0.25	7.80
0.5	0.5	0.5	15.6
0.75	0.75	0.75	23.4
1.0	1.0	1.0	31.2

and 313 K. The positive temperature dependence of IE suggests that the inhibitive action was not weakened by thermal activation; on the contrary, higher temperatures appeared to promote the effectiveness of the inhibitor. Such behavior is commonly associated with an adsorption process that is endothermic in nature and becomes more favorable at elevated temperatures, leading to a higher surface coverage and/or stronger interaction between inhibitor species and the aluminum surface.

Thus, the gradual decrease in CR and concomitant increase in IE with concentration indicate the formation of an increasingly compact interfacial layer that hindered the access of aggressive ions and retarded charge transfer across the metal/solution interface[36].

Activation energy (E_a) values were evaluated with the logarithmic form of the Arrhenius equation as follows[37]:

$$\log \mathrm{CR} = \log A - \frac{E_a}{2.303RT} \quad (6)$$

where A is the Arrhenius pre-exponential factor, T is absolute temperature (K), and R is universal gas constant (8.314 J mol^{-1} K^{-1}). The plots of log CR against $1/2.303RT$ are linear with slope corresponding to $-E_a$ and intercept corresponding to log$A$.

Enthalpy (ΔH^*, kJ mol^{-1}) and entropy (ΔS^*, J mol^{-1} K^{-1}) of activation were obtained from the slope $-\Delta H^*/2.303R$ and intercept [log$R$/Nh + ($\Delta S^*/2.303R$)], respectively, from the plot of log-CR/T versus $1/T$ in accordance with the following alternative form of Arrhenius equation (7):

$$\log\frac{\mathrm{CR}}{T} = \frac{-\Delta H^*}{2.303R}\left(\frac{1}{T}\right) + \left[\log\frac{R}{\mathrm{N_A h}} + \left(\frac{\Delta S^*}{2.303R}\right)\right] \quad (7)$$

where h is Planck's constant, $\mathrm{N_A}$ is Avogadro's number, CR is the corrosion rate, T is thermodynamic temperature, R is the universal gas constant, ΔS^* is the entropy change, and ΔH^* is the enthalpy change[38].

Graphical representation of activation parameters determined from the Arrhenius plots and transition state plots in accordance with Eqs. 6 and 7 are presented in Fig. 4.

Table 5 presents the activation parameters for the corrosion of D16T aluminum alloy in model FW in the absence and presence of varying concentrations of the BNP inhibitor.

The Arrhenius plots (Fig. 4a) exhibited good linearity over the investigated temperature range ($R^2 \approx 0.99$), indicating that the dissolution process followed an activated behavior and that a single dominant kinetic regime operated. The apparent activation energy (E_a) decreased systematically from 76.45 kJ mol^{-1} for the uninhibited solution to 42.29 kJ mol^{-1} at the highest BNP concentration (31.2 mg dm^{-3}). Such a reduction in E_a in the presence of the inhibitor suggests that the corrosion process proceeded through an alternative, energetically more favorable pathway when the metal surface was covered by the inhibitor film. In line with common interpretations, this trend is consistent with the formation of an adsorbed protective layer whose stability increased with concentration[39].

Regarding the pre-exponential factor (log A), Table 5 shows a pronounced and systematic decrease from 14.83 for the blank solution to 8.56 at 31.2 mg dm^{-3} of BNP inhibitor. Since the Arrhenius constant A reflects the number of effective collisions leading to metal dissolution, its reduction in-

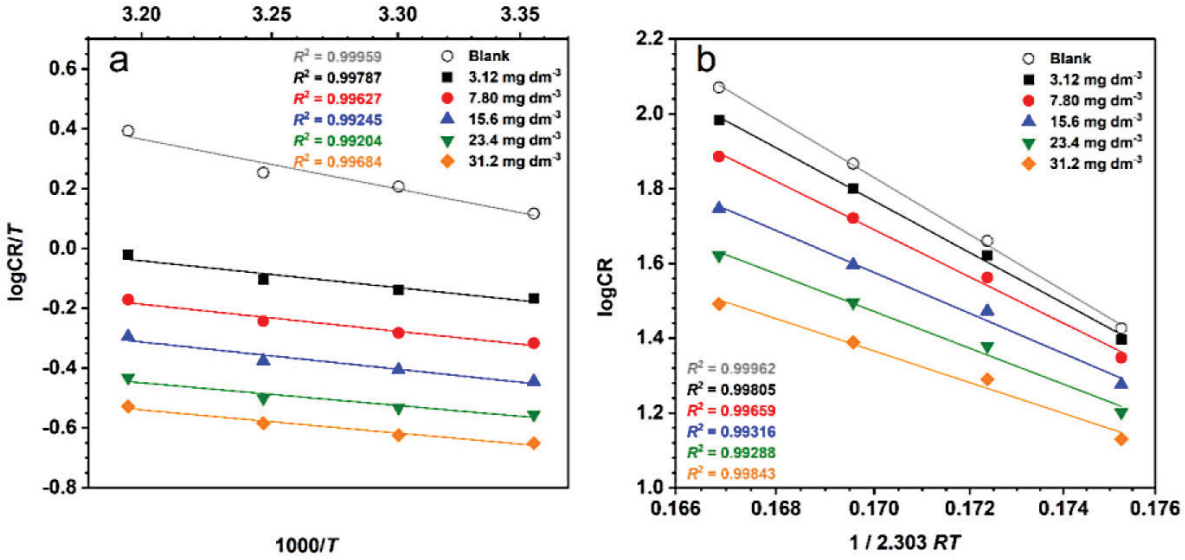

Fig. 4 – *Arrhenius plots (a) and transition state plots (b) for D16T aluminum alloy in model FW in the absence and presence of BNP inhibitor at different concentrations after 2 hours of immersion*

Table 5 – *Activation parameters for the dissolution of D16T aluminum alloy in model FW in the absence and presence of varying concentrations of the BNP inhibitor*

Concentration, mg dm^{-3}	log$A$	E_a, kJ mol^{-1}	ΔH^*, kJ mol^{-1}	ΔS^*, J mol^{-1} K^{-1}
Blank	14.83	76.45	4.96	–138.49
3.12	13.55	69.31	5.48	–139.18
7.80	12.46	63.33	6.01	–140.02
15.6	10.90	54.85	6.96	–141.57
23.4	9.84	49.22	7.79	–143.14
31.2	8.56	42.29	9.10	–145.43

dicates a substantial decrease in the probability that activated species reached the appropriate configuration for electron transfer at the metal/solution interface[40].

In kinetic terms, the simultaneous decrease of both E_a and log A suggests that the inhibitor does not merely modify the energetic barrier but also strongly affects the entropic and steric factors governing the corrosion process. The lower A values in the inhibited systems are consistent with a reduced number of available active sites and a restriction of the degrees of freedom of reacting species due to surface coverage by the inhibitor layer[41].

From a mechanistic standpoint, the decrease in log A can therefore be attributed to the blocking and reorganization of interfacial sites by adsorbed BNP inhibitor molecules, leading to a lower frequency of successful metal–solution encounters[42]. However, as with the activation parameters, this conclusion is only based on kinetic–thermodynamic correlations.

The transition state plots (Fig. 4b) also show excellent linear correlations, allowing reliable determination of the enthalpy (ΔH^*) and entropy (ΔS^*) of activation. The positive values of ΔH^* (4.96–9.10 kJ mol^{-1}) confirm the endothermic character of the metal dissolution step, while the gradual increase in ΔH^* with inhibitor concentration implies a higher energy requirement for the formation of the activated complex in the inhibited system, reflecting the additional energy needed to disrupt the adsorbed layer prior to charge transfer[43].

Moreover, the entropy of activation was negative for all systems and became more negative as the BNP inhibitor concentration increased (from −138.49 to −145.43 J mol^{-1} K^{-1}). This indicates that the activated state was more ordered than the initial state, which is commonly associated with an associative or constrained transition state[44]. The decreasing magnitude of ΔS^* in the presence of the inhibitor may be attributed to a more organized interfacial environment, plausibly arising from the structured arrangement of inhibitor molecules and solvent at the metal/solution interface.

The outcome of the combined Arrhenius and transition-state analyses led to the conclusion that the BNP inhibitor significantly altered the kinetic and thermodynamic parameters of D16T aluminum alloy dissolution in model FW. The concentration-dependent decrease in E_a, together with the systematic variations in ΔH^* and ΔS^*, is consistent with a corrosion process controlled by surface coverage and interfacial reorganization. These findings strongly support an adsorption-mediated inhibition mechanism.

Adsorption isotherms and thermodynamic parameters

Most organic inhibitors are adsorbed onto a metal surface by displacing water molecules and forming a barrier. The efficiency of the inhibitor depends on the stability of the chelate formed, which in turn depends on the type and nature of the inhibitor molecule[45].

Adsorption of an inhibitor onto a metal surface may have a chemical, physical, or mixed nature. To gain insight into the adsorption mechanism, the values of ΔG^0_{ads} should be determined. The ΔG^0_{ads} values up to –20 kJ mol^{-1} indicate electrostatic interaction between the metal surface and the charged inhibitor molecules (physiosorption). Values around –40 kJ mol^{-1} are usually considered as a threshold between chemisorption and physiosorption, or less indicate the chemical nature of sorption[46]. This involves electron transfer from the organic molecule to the metal surface with the formation of a coordination-type bond. To elucidate the adsorption mechanism of BNP inhibitor on the D16T aluminum alloy surface, the Langmuir, Freundlich, Temkin, Frumkin, El-Awady, and Flory-Huggins adsorption models were applied in accordance with their respective mathematical expressions[47]. The values of K_{ads} obtained from the isotherms were used to calculate the Gibbs free energy according to the known relationship[48]:

$$\Delta G^0_{ads} = -RT\ln(1000K_{ads}) \quad (8)$$

where ΔG^0_{ads} is the Gibbs free energy of adsorption, R is the universal gas constant, T is the thermodynamic temperature, and 1000 is the concentration of water in g dm^{-3}.

The adsorption isotherms describing the behavior of the BNP inhibitor on the D16T aluminum alloy surface in model FW at 298–313 K are shown in Fig. 5.

The obtained plots are almost linear with correlation coefficients (R^2) ranging from 0.95331 to 0.99751. Adsorption parameters obtained from isotherms are listed in Table 6.

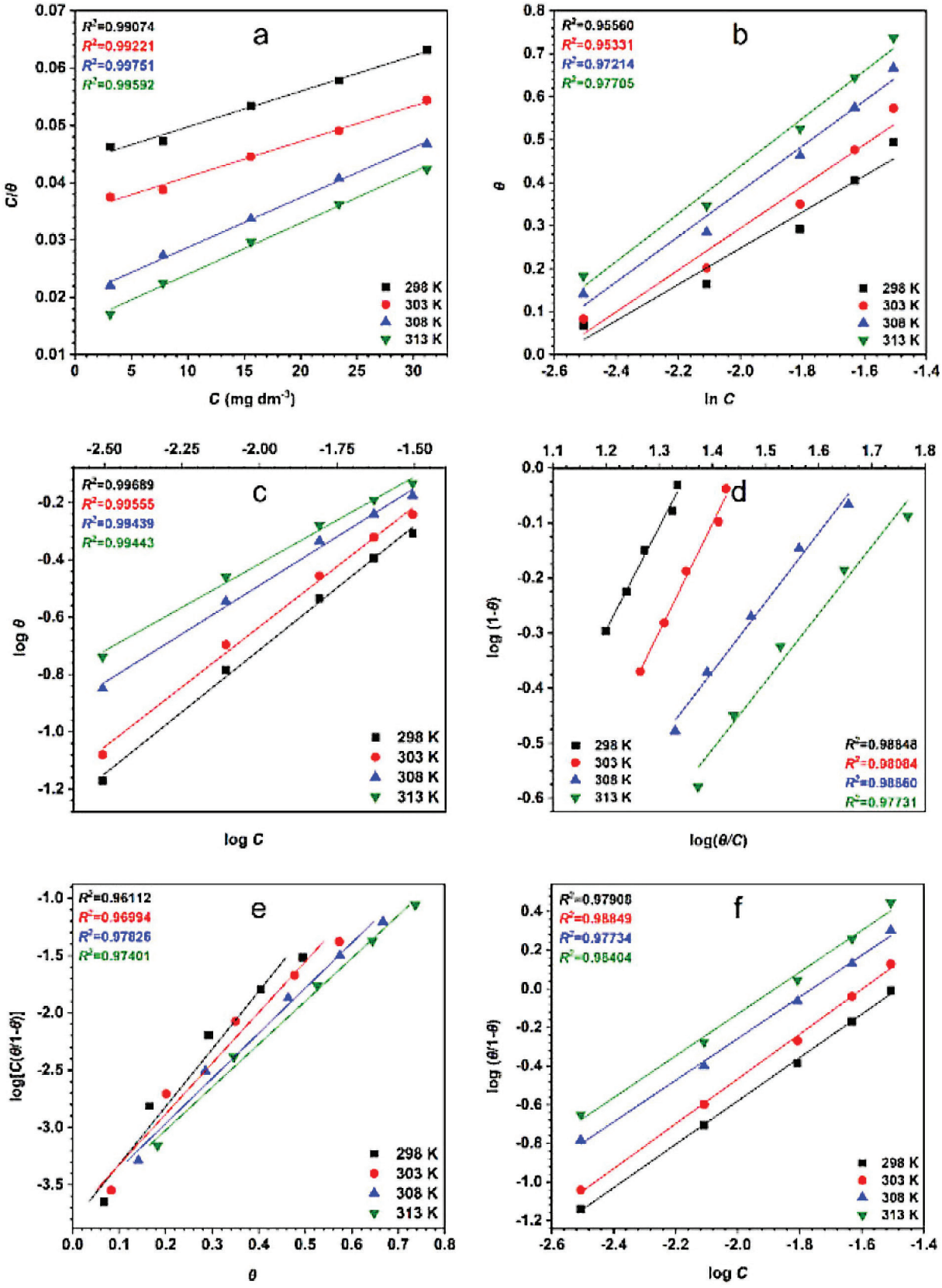

Fig. 5 – *Adsorption isotherms for BNP inhibitor on D16T aluminum alloy surface in model FW: Langmuir (a), Temkin (b), Freundlich (c), Flory-Huggins (d), Frumkin (e), El-Awady (f)*

Table 6 – *Parameters for adsorption of BNP inhibitor containing H_3BO_3 ($1\cdot10^{-4}$ mol dm^{-3}), 1,4-PDA ($1\cdot10^{-4}$ mol dm^{-3}), and Na_2HPO_4 ($1\cdot10^{-4}$ mol dm^{-3}) on D16T aluminum alloy surface in model FW*

Isotherm	*T*, K	Slope	Intercept	R^2	K_{ads}, dm^3 g^{-1}	ΔG^0_{ads}, kJ mol^{-1}	Isotherm property
Langmuir	298	0.62014	0.04353	0.99074	22.97	–24.88	–
	303	0.61895	0.03482	0.99221	28.72	–25.86	–
	308	0.87105	0.01998	0.99751	50.05	–27.71	–
	313	0.86448	0.01536	0.99592	65.10	–28.85	–
Temkin	298	0.42121	1.08977	0.95560	1.09	–17.33	–
	303	0.48607	1.26607	0.95331	1.27	–18.00	–
	308	0.52668	1.43309	0.97214	1.43	–18.61	–
	313	0.55421	1.54669	0.97705	1.55	–19.11	–
							n
Freundlich	298	0.86626	1.01826	0.99689	10.43	–22.93	1.15
	303	0.84023	1.04703	0.99555	11.14	–23.48	1.19
	308	0.67849	0.86790	0.99439	7.38	–22.81	1.47
	313	0.60785	0.80171	0.99443	6.33	–22.78	1.65
							b
Flory-Huggins	298	1.87161	–2.54022	0.98848	0.00288	–2.62	1.87
	303	1.96690	–2.85486	0.99084	0.00140	–0.84	1.97
	308	1.26195	–2.13707	0.98860	0.00729	–5.09	1.26
	313	1.23144	–2.23544	0.97731	0.00582	–4.58	1.23
							α
Frumkin	298	0.19899	0.76083	0.96112	2.14	–19.00	0.099
	303	0.22569	0.85058	0.96994	2.34	–19.55	0.113
	308	0.25413	0.95347	0.97826	2.59	–20.13	0.127
	313	0.26684	1.00675	0.97401	2.74	–20.60	0.133
							y
El-Awady	298	0.88998	–1.48286	0.97908	0.0739	–10.66	0.445
	303	0.86030	–1.59809	0.98849	0.0587	–10.26	0.430
	308	0.92501	–1.76094	0.97734	0.0375	–9.28	0.463
	313	0.91825	–1.87927	0.98404	0.0288	–8.74	0.459

As can be seen, the Langmuir and Freundlich isotherms show the highest and most consistent R^2 values (≥0.99) among other models, suggesting that they provide the most appropriate description of the adsorption process.

Obeying the Langmuir model indicates that adsorption proceeded predominantly through the formation of a surface layer in which each inhibitor entity occupied a defined number of active sites, and that, within the investigated concentration range, the coverage approached monolayer-type behavior[49]. This suggests that the adsorption process was governed mainly by site saturation and that, on average, each adsorption site accommodated one adsorbed species without the need to invoke multilayer formation[50]. The absence of significant deviation from linearity also implies that lateral interactions between adsorbed molecules did not dominate the adsorption equilibrium under the given conditions[51].

Simultaneously, the good fit with the Freundlich isotherm reflects the energy heterogeneity of the D16T aluminum alloy surface and the non-uniform distribution of adsorption energies. This model accounts for the existence of sites with different affinities, which is consistent with a real alloy surface[52].

When considered as a whole, the combined validity of the Langmuir and Freundlich adsorption models suggests that the BNP inhibitor components adsorbed mainly as a monolayer on the D16T aluminum alloy surface, while the adsorption energy was not strictly uniform but distributed over surface sites[53]. Thus, the adsorption of BNP inhibitor on metal surface may be described as monolayer-type on energetically heterogeneous sites.

The negative values of ΔG^0_{ads} indicate that the adsorption of the BNP inhibitor on the D16T aluminum surface was a spontaneous process over the investigated temperature range[54]. The range of ΔG^0_{ads} (from −25 to −29 kJ mol^{-1}) reflects a sufficiently strong affinity between the inhibitor molecules and the surface to ensure stable surface coverage, which is consistent with the good conformity to monolayer-type Langmuir behavior[55].

Within the framework of the Langmuir model, the increasingly negative ΔG^0_{ads} with temperature was associated with an increase in the adsorption equilibrium constant, implying that the formation of the adsorbed layer became thermodynamically more favorable as thermal activation facilitated surface accommodation of the inhibitor species. In the context of the Freundlich model, the negative ΔG^0_{ads} values likewise confirm that adsorption on a heterogeneous set of sites was energetically favorable, while the spread of adsorption energies implied by this model was compatible with a distribution of local free energies of interaction rather than a single uniform value.

However, the absolute values of ΔG^0_{ads} are in a range often attributed as the boundary between physisorption and chemisorption, and the final determination of the adsorption nature cannot be made for purely thermodynamic reasons. Therefore, the obtained Gibbs free energy data should be interpreted as evidence of spontaneous and relatively strong adsorption, supporting the formation of a stable, predominantly monolayer-type protective film on an energetically heterogeneous D16T aluminum alloy surface.

The values of ΔH^0_{ads} and ΔS^0_{ads} were determined from the obtained values of ΔG^0_{ads} using the rearranged Gibbs-Helmholtz equation as follows:

$$\Delta G^0_{ads} = \Delta H^0_{ads} - T\Delta S^0_{ads} \quad (9)$$

The slope and intercept of the ΔG^0_{ads} versus T plot allow determination of the values of ΔS^0_{ads} and ΔH^0_{ads}, respectively (Fig. 6).

The positive enthalpy of adsorption ΔH^0_{ads} (57.13 kJ mol^{-1}) indicates that the adsorption of the inhibitor was an endothermic process, implying that effective surface coverage was thermodynamically favored at higher temperatures. This suggests that thermal activation facilitated the adsorption step, likely by promoting the intensive displacement of pre-adsorbed solvent and enabling the inhibitor molecules to access and occupy surface sites[56].

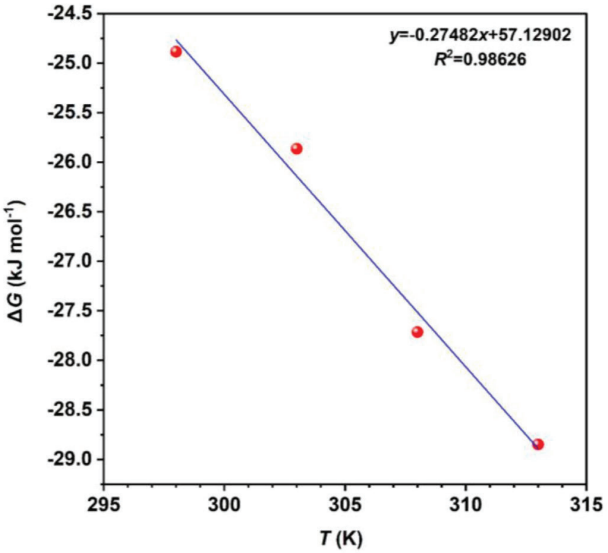

Fig. 6 – *Relationship between Gibbs free energy (ΔG^0_{ads}) and absolute temperature (T) for D16T aluminum alloy in model FW*

The positive entropy of adsorption ΔS^0_{ads} (274.82 J mol^{-1} K^{-1}) reflects an increase in disorder upon adsorption. This can be rationalized by considering the interfacial exchange process, in which several water molecules, initially coordinated to the metal surface, were released into the bulk solution when an inhibitor molecule became adsorbed[32]. The gain in translational and configurational freedom of the displaced solvent molecules outweighs the ordering associated with the fixation of the inhibitor at the surface, resulting in a net positive entropy change. The positive values of both ΔH^0_{ads} and ΔS^0_{ads} are therefore consistent with an entropy-driven adsorption process that becomes increasingly favorable with increasing temperature[57].

Electrochemical measurements

To confirm the effectiveness of the developed inhibitor, electrochemical studies were conducted.

To determine the stability of the assembled film over the metal surface, CA measurements were performed. For this purpose, 50.0 mV anodic or cathodic overpotentials (E_{corr} ± 50.0 mV) were applied to the system for 1800 s and the current densities observed were plotted against operation time. As a reference, similar measurements were also performed with a blank solution.

The electrochemical performance of the BNP inhibitor on D16T aluminum alloy in model FW was evaluated using open-circuit potential (OCP), potentiodynamic polarization, chronoamperometric, and chronopotentiometric measurements as given in Fig. 7.

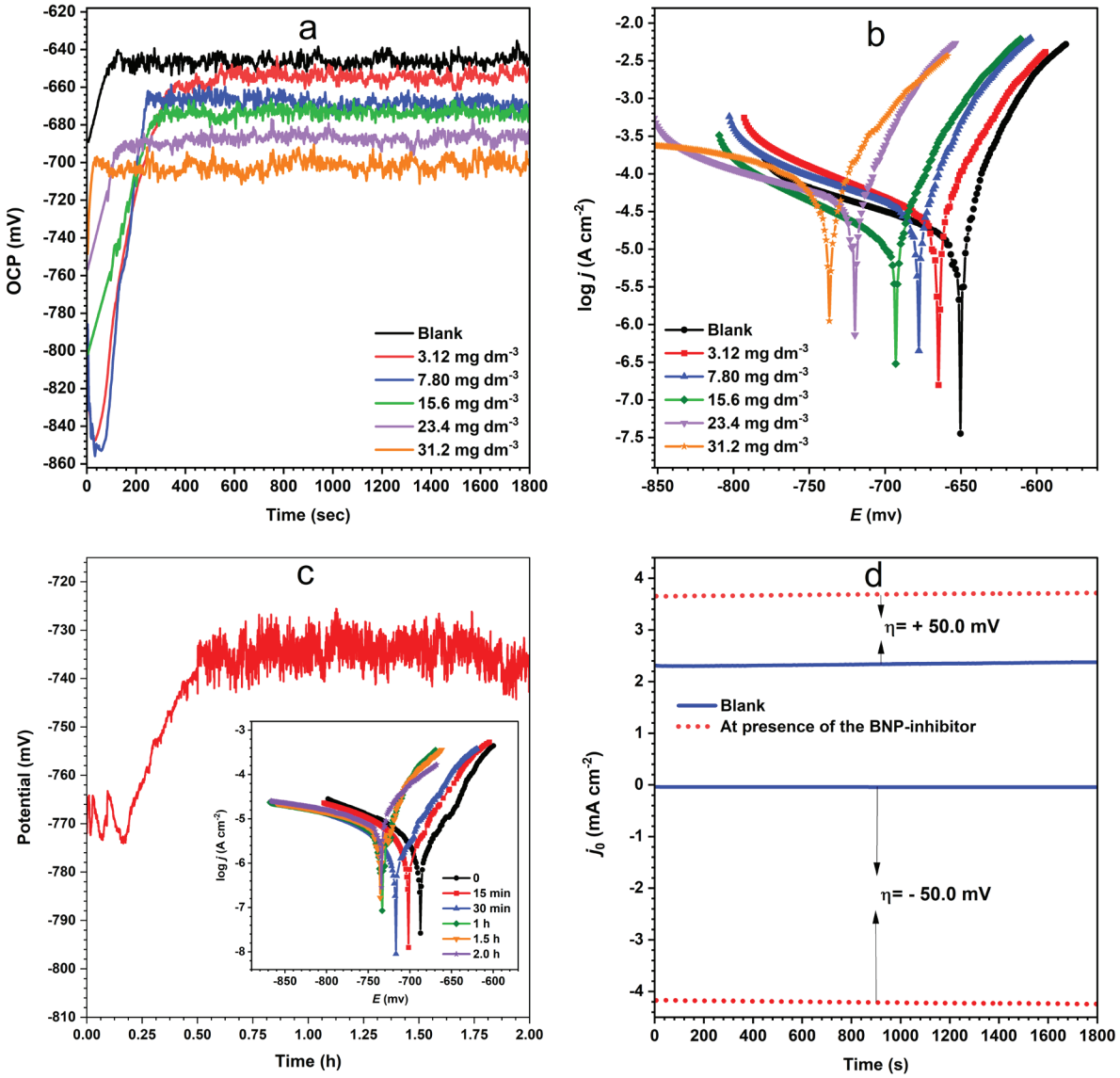

Fig. 7 – *Open-circuit potential (a), Tafel polarization (b), chronopotentiometric (c), and (d) chronoamperometric curves for D16T aluminum alloy in model FW containing various concentrations of the BNP inhibitor*

The corresponding electrochemical parameters are summarized in Table 7.

Fig. 7a illustrates the evolution of the open-circuit potential (OCP) of the D16T aluminum alloy in model FW in the absence and presence of different concentrations of the BNP inhibitor over a 30 min immersion period. In all cases, the OCP exhibited a rapid initial shift during the first few minutes of immersion, followed by a gradual stabilization, indicating the establishment of a quasi-steady interfacial state. In the uninhibited solution, the OCP stabilized at approximately −644 mV after an initial transient period, indicating the establishment of a steady interfacial state between the D16T aluminum alloy surface and the corrosion medium. Upon the addition of the inhibitor, the OCP progressively shifted toward more negative values, reaching approximately −703 mV at the highest inhibitor concentration investigated. Such negative displacement of the OCP in the presence of the inhibitor for aluminum, particularly in chloride-containing acidic media, are frequently associated with changes in the relative kinetics of anodic and cathodic reactions[58]. The observed progressive stabilization of OCP over time further indicates that the aluminum surface reached a quasi-equilibrium condition, associated with the formation of a relatively stable adsorbed inhibitor layer, which altered charge transfer at the metal/solution interface[59]. Moreover, for aluminum alloys, inhibition is frequently associated with a suppression of localized cathodic activity rather than a simple blocking of anodic sites[60]. In this context, a negative OCP shift may arise from a relative reduction in cathodic reaction kinetics, particularly hydrogen evolution or oxygen reduction, which can dominate the mixed potential in acidic chloride me-

Table 7 – *Potentiodynamic polarization parameters for the corrosion of D16T aluminum alloy in model FW in the absence and presence of different concentrations of BNP inhibitor*

Concentration, mg dm^{-3}	OCP, mV	E_{corr}, mV	j_{corr}, A cm^{-2}	IE$_j$, %	R_p, Ω	IE$_R$, %
Blank	–643.87	–658.68	$6.41\cdot10^{-6}$	–	1975.3	–
3.12	–658.12	–667.83	$5.74\cdot10^{-6}$	10.50	2489.4	20.65
7.80	–669.55	–676.57	$5.45\cdot10^{-6}$	15.08	3258.3	39.38
15.6	–675.36	–691.13	$4.06\cdot10^{-6}$	36.66	4516.4	56.26
23.4	–689.40	–719.18	$3.58\cdot10^{-6}$	44.26	5853.6	66.25
31.2	–702.97	–733.90	$2.16\cdot10^{-6}$	66.39	6721.2	70.61

dia[61]. This interpretation is supported by the simultaneous decrease in corrosion current density and the increase in the polarization resistance (Table 7), which indicate a general decrease in corrosion activity.

Representative potentiodynamic polarization curves recorded in the absence and presence of different inhibitor concentrations are shown in Fig. 7b, while the corresponding electrochemical parameters are summarized in Table 7. The addition of the inhibitor resulted in a marked decrease in the corrosion current density (j_{corr}), from $6.41\cdot10^{-6}$ A cm^{-2} for the blank solution to $2.16\cdot10^{-6}$ A cm^{-2} at the highest inhibitor concentration. This pronounced reduction in j_{corr} clearly indicates an effective suppression of the corrosion rate signifying that the inhibitor molecules have adsorbed onto the metal surface and are hindering the electrochemical reactions responsible for corrosion[62]. As can be seen, both the anodic and cathodic branches of the polarization curves were affected by the presence of the inhibitor. Moreover, the shift in corrosion potential (E_{corr}) relative to the uninhibited system remained below 85 mV, suggesting that the inhibitor can be classified as a mixed-type inhibitor[63]. This behavior implies that the inhibitor influenced both metal dissolution and cathodic reactions, although the exact extent of its effect on each partial process cannot be unequivocally quantified from polarization data alone, particularly for aluminum systems where passive film formation may affect the linearity of Tafel curves[64]. The inhibition efficiency calculated from polarization measurements increased with inhibitor concentration, reaching approximately 66 %, which is consistent with effective surface coverage and progressive blocking of active corrosion sites.

The chronopotentiometric curves recorded at a constant applied current density (Fig. 7c) provide additional insight into the time-dependent electrochemical behavior of the D16T aluminum alloy surface. In the presence of the inhibitor, the potential rapidly reached a stable value and remained nearly constant throughout the measurement period. This enhanced potential stability suggests that the inhibitor contributed to the formation of a more uniform and persistent surface condition[65]. The inset polarization responses further indicate that the inhibited system exhibited reduced electrochemical activity, consistent with the development of a protective interfacial layer. While these observations support an adsorption-controlled inhibition process, they do not, by themselves, distinguish between physical and chemical adsorption mechanisms[66].

Chronoamperometric measurements conducted at a fixed overpotential of ±50 mV (Fig. 7d) revealed a significant decrease in current density in the presence of the inhibitor compared to the blank solution. Notably, the current remained relatively stable over time, with no evidence of a progressive increase that would indicate surface degradation or breakdown of the protective layer. The reduced and stabilized current response suggests that the inhibitor effectively limited charge transfer processes at the metal–solution interface. The stable low current also indicates that the inhibitor had formed a robust and persistent film that maintained its integrity and protective properties under the constant electrochemical stress of the applied potential[67]. This behavior is consistent with the formation of an adsorbed inhibitor film that acts as a barrier to both anodic metal dissolution and cathodic reactions[68].

The obtained electrochemical results clearly demonstrate that the inhibitor markedly enhanced the corrosion resistance of aluminum in the investigated medium. The observed trends are mutually consistent and collectively indicate that the inhibition process was predominantly controlled by surface adsorption and interfacial modification. This internal consistency among the electrochemical parameters provides strong evidence for the effective corrosion inhibition performance of the studied system.

Contact angle measurements

Fig. 8 displays the values of the contact angles for the D16T aluminum alloy surface both with and without the inhibitor, taken before and after immersion in model FW.

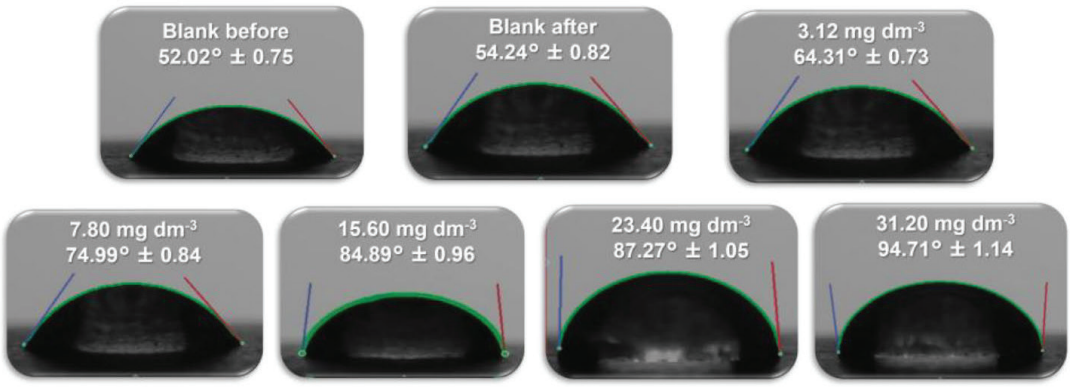

Fig. 8 – *Contact angle values before and after immersing the D16T aluminum alloy in model FW in the presence of varying BNP-inhibitor concentrations*

The contact angle results reveal the effect of the BNP inhibitor on the surface wettability of the D16T aluminum alloy in model FW. The untreated alloy exhibited a contact angle of 52.02º ± 0.75, which slightly increased to 54.24º ± 0.82 after immersion in model FW without inhibitor, reflecting minor surface changes due to corrosion products. In contrast, the addition of BNP inhibitor significantly increased the contact angle, reaching 64.31º ± 0.73 at 3.12 mg dm^{-3} and 94.71º ± 1.14 at 31.20 mg dm^{-3}. This gradual increase indicates efficient adsorption of the inhibitor molecules, resulting in a compact hydrophobic layer which limited the interaction between the metal and the corrosion medium. Enhanced hydrophobicity confirms the barrier-type protection mechanism of the BNP inhibitor, where the adsorbed film prevented the entry of aggressive ions and water molecules onto the metal surface[69].

Conclusion

This study demonstrates that the novel ternary BNP inhibitor provides highly efficient corrosion protection for D16T aluminum alloy in synthetic formation water, confirming the effectiveness of multicomponent inhibition systems. The combined presence of boric acid, 1,4-phenylenediamine, and disodium hydrogen orthophosphate significantly enhanced protective performance compared with mono- and binary-component systems, indicating cooperative interactions between the inhibitor constituents. The boric acid–orthophosphate binary system exhibited inhibition efficiencies close to those of the ternary formulation, suggesting that these components play a dominant role in protective film formation, whereas 1,4-phenylenediamine likely contributes to improved surface coverage and stabilization of the protective layer. Electrochemical and gravimetric measurements consistently revealed a pronounced reduction in corrosion rate, accompanied by increased polarization resistance and decreased corrosion current density. Thermodynamic and kinetic analyses indicated that adsorption occurred spontaneously and was thermodynamically favorable. The positive enthalpy and entropy values suggest adsorption accompanied by interfacial reorganization and partial displacement of water molecules, while the increasing stability of the adsorbed layer with temperature may indicate a gradual contribution of stronger surface interactions. Contact angle measurements confirmed increased surface hydrophobicity, supporting the formation of a barrier-type protective layer. Polarization data suggest mixed-type inhibition affecting both anodic and cathodic reactions. These findings provide a mechanistic framework for the rational development of multicomponent inhibitors for aluminum alloys operating in aggressive oil and gas production environments.

ACKNOWLEDGMENTS

The authors gratefully acknowledge the Head and staff of the Laboratory of Ecology and Biogeochemistry, M. Utemisov West Kazakhstan University, for providing the facilities, technical support, and assistance necessary to conduct this research.

CONFLICTS OF INTEREST

The authors declare that they have no conflicts of interest, whether financial or personal, that could have influenced the results or interpretation of this work.

References

1. *Aslam, R., Mobin, M., Aslam, J.,* Corrosion inhibitors for refinery industries, in Hussain, C. Verma, C. and Aslam, J. (Eds.), Environmentally Sustainable Corrosion Inhibitors, Elsevier, 2022, pp 385–404.
doi: https://doi.org/10.1016/B978-0-323-85405-4.00004-5

2. *Solovyeva, V. A., Almuhammadi, K. H., Badeghaish, W. O.,* Current downhole corrosion control solutions and trends in the oil and gas industry: A review, Materials **16** (2023) 1795.
doi: https://doi.org/10.3390/ma16051795
3. *Zheng, Z., Hu, J., Eliaz, N., Zhou, L., Yuan, X., Zhong, X.,* Mercaptopropionic acid-modified oleic imidazoline as a highly efficient corrosion inhibitor for carbon steel in CO_2-saturated formation water, Corros. Sci. **194** (2022) 109930.
doi: https://doi.org/10.1016/j.corsci.2021.109930
4. *Divya, Kriti, S., Shweta, M.,* A review on composition and mechanical strength of wrought aluminum alloy series, IJERMCE **9** (2022) 12.
5. *Georgantzia, E., Kashani, M. M.,* On the use of aluminium alloys in sustainable design, construction and rehabilitation of bridges, Proc. Inst. Civ. Eng. Bridg. Eng. **178** (2024) 229.
doi: https://doi.org/10.1680/jbren.23.00018
6. *Calderón, J. P., Reyes Barragán, J. L., Barraza Fierro, J. I., Cruz Mejía, H., Arrieta González, C. D., Ravelero Vázquez, V.,* Corrosion behavior of Al modified with Zn in chloride solution, Materials **15** (2022) 4229.
doi: https://doi.org/10.3390/ma15124229
7. *Ahmed, E., Liu, J., Liu, J.,* Mitigating corrosion in downhole environments of oil and gas operations: Mechanisms, challenges, and control strategies, Trends Sci. **22** (2025) 9855.
doi: https://doi.org/10.48048/tis.2025.9855
8. *Feder, J.,* Reuse of produced water grows in the oil and gas industry, J. Pet. Technol. **72** (2020) 60.
doi: https://doi.org/10.2118/1220-0060-JPT
9. *Stefanakis, A. I., Prigent, S., Breuer, R.,* Integrated produced water management in a desert oilfield using wetland technology and innovative reuse practices, in Stefanakis, A. (Ed.), Constructed Wetlands for Industrial Wastewater Treatment, John Wiley & Sons, Hoboken, 2018, pp 23–42.
doi: https://doi.org/10.1002/9781119268376.ch1
10. *Hardi, M., Siregar, Y. I., Anita, S., Ilza, M.,* Determination of heavy metals concentration in produced water of oil field exploration in Siak regency, J. Phys. Conf. Ser. **1156** (2019) 012009.
doi: https://doi.org/10.1088/1742-6596/1156/1/012009
11. *Abou El Leil, I. M., El Mezweghy, A. M., Haman, E. A.,* Classification and geological environment identification of produced water in oilfields, Int. Sci. Technol. J. **30** (2022) 1.
12. *Mammadova, N. I.,* Ecological management of characteristics of formation waters from flooded deposits, J. Geol. Geogr. Geoecol. **33** (2024) 319.
doi: https://doi.org/10.15421/112430
13. *Carlos, M., Menendez, O., Mazyar, R., Ramachandran, S., Jackson, T.,* Identification of synergistic interactions in green corrosion inhibitor mixtures by molecular modeling, Corrosion **80** (2024) 1109.
doi: https://doi.org/10.5006/4543
14. *Zhu, C., Yang, H. X., Wang, Y. Z.,* Synergistic effect between glutamic acid and rare earth cerium (III) as corrosion inhibitors on AA5052 aluminum alloy in neutral chloride medium, Ionics **25** (2019) 1395.
doi: https://doi.org/10.1007/s11581-018-2605-4
15. *Zhang, F., Wang, S., Fei, R., Geng, S., Huang, C., Zhao, B.,* Tailoring ionic liquid corrosion inhibitors for N80 steel in acidic media, Langmuir **41** (2025) 13315.
doi: https://doi.org/10.1021/acs.langmuir.5c01038
16. *Guo, Y., Jin, P., Shao, M., Dong, S., Du, R., Lin, C.,* Effect of an environmentally friendly diisooctyl sebacate-based mixed corrosion inhibitor on reinforcing steel, Acta Phys. Chim. Sin. (2020) 2003033.
doi: https://doi.org/10.3866/PKU.WHXB202003033
17. *Zhang, F., Wang, S., Fei, R., Geng, S., Huang, C., Zhao, B.,* Tailoring ionic liquid corrosion inhibitors for N80 steel in acidic media: Anion–cation synergy, high-temperature performance, and multiscale mechanistic insights, Langmuir **41** (2025) 13315.
doi: https://doi.org/10.1021/acs.langmuir.5c01038
18. *Parveen, M., Mobin, M., Zehra, S., Aslam, R.,* L-Proline mixed with sodium benzoate as sustainable inhibitor for mild steel corrosion in 1 M HCl, Sci. Rep. **8** (2018) 7489.
doi: https://doi.org/10.1038/s41598-018-24143-2
19. *Mékarbané, P., Alonzo, D., Moser, F., Larrouy, G.,* Development of combined corrosion and scale inhibitors, CORROSION 2019, NACE International, Nashville, 2019.
20. *Seilova, T., Kunasheva, Z., Kubasheva, R., Akatyev, N.,* Development of new three-component BNP inhibitor for carbon steel in 0.5 mol dm^{-3} HCl solution, Int. J. Corros. Scale Inhib. **13** (2024) 1268.
doi: https://doi.org/10.17675/2305-6894-2024-13-2-33
21. *Tsygankova, L. E., Vigdorovich, V. I., Shel, N. V., Dubinskaya, E. V.,* Peculiarities of protective efficiency of nitrogen containing inhibitors of steel corrosion, Int. J. Corros. Scale Inhib. **2** (2013) 304.
doi: https://doi.org/10.17675/2305-6894-2013-2-4-304-310
22. ISO 8407, Corrosion of metals and alloys – Removal of corrosion products from corrosion test specimens, ISO, Geneva, 2021.
23. *Akatyev, N., Khapiyeva, M., Kenzhegalieva, R., Talapova, A., Uzakbay, G., Tlektes, A., Logashkina, A.,* Investigation of *Prunus domestica* leaves aqueous extracts as corrosion inhibitor for carbon steel in 1 M HCl, J. Sci. Technol. **17** (2025) 64.
doi: https://doi.org/10.30880/jst.2025.17.02.006
24. *Muthamma, K., Kumari, P., Lavanya, M.,* Corrosion inhibition of mild steel in acidic media by N-[(3,4-dimethoxyphenyl)methyleneamino]-4-hydroxy-benzamide, J. Bio-Tribo-Corros. **7** (2021).
doi: https://doi.org/10.1007/s40735-020-00439-7
25. *Upadhya, H. S., Kshama, S. S., Vishwas, K. R., Swamynathan, K., Choudhuri, J. R., Rao, P. S.,* Benzoic acid-based supramolecular synthons as corrosion inhibitor, Can. Metall. Q. **64** (2025) 2065.
doi: https://doi.org/10.1080/00084433.2024.2431383
26. *Rao, S., Smitha Shree, Sowmyashree, A. S., Rao, P.,* Sodium hyaluronate as an effective eco-friendly corrosion inhibitor, Can. Metall. Q. **64** (2025) 1149.
doi: https://doi.org/10.1080/00084433.2024.2375465
27. *Rodič, P., Milosev, I., Frankel, G. S.,* Corrosion and protection of synthetic intermetallic compounds and bulk aluminum alloy, ECS Meet. Abstr. (2023) 1131.
doi: https://doi.org/10.1149/MA2023-02131131mtgabs
28. *Yasakau, K. A., Salak, A. N., Zheludkevich, M. L., Ferreira, M. G. S.,* Volta potential of oxidized aluminum studied by scanning Kelvin probe force microscopy, J. Phys. Chem. C **114** (2010) 8474.
doi: https://doi.org/10.1021/jp1011044
29. *Zin, I. M., Khlopyk, O. P.,* Repassivation of aluminum in the presence of phosphate and nitrate inhibitors, Mater. Sci. **50** (2015) 676.
doi: https://doi.org/10.1007/s11003-015-9771-6

30. *Ji, L., Chen, J., Zhang, R.,* Corrosion resistance of anodized 6463 aluminum alloy in 3.5 % sodium chloride solution, Int. J. Electrochem. Sci. **16** (2021) 211238. doi: https://doi.org/10.20964/2021.12.38
31. *Alamry, K. A., Khan, A., Aslam, J.,* Corrosion inhibition of mild steel in hydrochloric acid solution by expired ampicillin drug, Sci. Rep. **13** (2023) 6724. doi: https://doi.org/10.1038/s41598-023-33519-y
32. *Mubarak, G., Verma, C., Mazumder, M. A. J., Barsoum, I., Alfantazi, A.,* Exploring hydrophobic effects of quaternary ammonium copolymers on corrosion of casing steel, PLoS ONE **20** (2025) e0320981. doi: https://doi.org/10.1371/journal.pone.0320981
33. *El-Aouni, N., Dagdag, O., El Amri, A.,* New hexafunctional epoxy prepolymer: Innovation structure for corrosion inhibition, J. Bio-Tribo-Corros. **10** (2024). doi: https://doi.org/10.1007/s40735-024-00844-2
34. *Ede, U. B., Ukpai, N. F., Nwofe, P. A., Jacintha, I. B., Nelson, N. E., Ficus ottoniifolia* leaf extract as green corrosion inhibitor for mild steel, World J. Adv. Res. Rev. **29** (2026) 206. doi: https://doi.org/10.30574/wjarr.2026.29.1.4297
35. *Al-Amiery, A. A., Isahak, W. N. R. W., Al-Azzawi, W. K.,* Corrosion inhibitors: Natural and synthetic organic inhibitors, Lubricants **11** (2023) 174. doi: https://doi.org/10.3390/lubricants11040174
36. *Mei, H., Zhou, B., Hu, S., Wu, C., Cen, H.,* Extract of photinia leaves as an effective corrosion inhibitor of carbon steel in 1 M HCl solution, J. Adhes. Sci. Technol. **39** (2025) 2384. doi: https://doi.org/10.1080/01694243.2025.2503245
37. *Kavimani, V., Gopal, P. M., Seikh, A. H., Abdo, H. S., Alnaser, I.,* Evaluation of anti-corrosion potential of *Parthenium hysterophorus* plant extract on AZ31 Mg alloy upon sodium chloride exposure, Can. Metall. Q. **64** (2025) 2128. doi: https://doi.org/10.1080/00084433.2024.2439159
38. *Toghan, A., Gadow, H. S., Fawzy, A., Alhussain, H., Salah, H.,* Adsorption mechanism, kinetics, thermodynamics, and anticorrosion performance of a new thiophene derivative for C-steel in a 1.0 M HCl: Experimental and computational approaches, Metals **13** (2023) 1565. doi: https://doi.org/10.3390/met13091565
39. *Emran, K. M., Omar, I. M. A., Arab, S. T., Ouerfelli N.,* On the pseudo-hyperbolic behavior of charge transfer resistance–temperature dependence in corrosion behavior of nickel-based glass alloy, Sci. Rep. **12** (2022) 6432. doi: https://doi.org/10.1038/s41598-022-10462-y
40. *Emembolu, L., Igwegbe, C.,* Investigation of temperature correlations on corrosion inhibition of carbon steel in acid media by flower extract, EJEAS **5** (2022) 29. doi: https://doi.org/10.55581/ejeas.1127813
41. *Katada, N., Sota, S., Morishita, N., Okumura, K., Niwa, M.,* Relationship between activation energy and pre-exponential factor normalized by the number of Brønsted acid sites in cracking of short chain alkanes on zeolites, Catal. Sci. Technol. **5** (2015) 1864. doi: https://doi.org/10.1039/C4CY01483A
42. *Corro, G., Torralba, R., Pal, U., Olivares-Xometl, O., Fierro, J. L. G.,* Total oxidation of methane over Pt/Cr_2O_3 catalyst at low temperature: Effect of Pt^0–Pt^{x+} dipoles at the metal–support interface, J. Phys. Chem. C. **123** (2019) 2882. doi: https://doi.org/10.1021/acs.jpcc.8b09748
43. *Okewale, A., Adesina, O.,* Kinetics and thermodynamic study of corrosion inhibition of mild steel in 1.5 M HCl medium using cocoa leaf extract as inhibitor, J. Appl. Sci. Environ. Manag. **24** (2020) 37. doi: https://doi.org/10.4314/jasem.v24i1.6
44. *El-Gendy, N. Sh., Hamdy, A., Omran, B. A.,* Thermal and surface studies on the corrosion inhibition of petroleum pipeline by aqueous extract of *Allium cepa* skin under acidic condition, Energy Sources A: Recovery Util. Environ. Eff. **40** (2018) 905. doi: https://doi.org/10.1080/15567036.2018.1465488
45. *Kadhim, A., Al-Amiery, A. A., Alazawi, R., Al-Ghezi, M. K. S., Abass, R. H.,* Corrosion inhibitors. A review, Int. J. Corros. Scale. Inhib. **10** (2021) 54. doi: https://doi.org/10.17675/2305-6894-2021-10-1-3
46. *Gong, M., Jiang, C., Zheng, X., Zeng, X., Lin, X.,* Corrosion inhibition of carbon steel in sulfuric acid by [BMIm] [Lys] amino acid ionic liquids, Adv. Mat. Res. **476** (2012) 1434. doi: https://doi.org/10.4028/www.scientific.net/AMR.476-478.1434
47. *Popoola, L. T.,* Organic green corrosion inhibitors (OGCIs): A critical review, Corros. Rev. **37** (2019) 71. doi: https://doi.org/0.1515/corrrev-2018-0058
48. *Zouied, D., Khelfaoui, M., Bouzenad, N., Abdennouri, A., Rouainia, M., Dob, K., Pulicaria odora* ethanolic extract as a corrosion inhibitor and its eco-friendly synthesis of CuO nanoparticles for photocatalytic and microbial properties, Chem. Biochem. Eng. Q. **39** (2025) 157. doi: https://doi.org/10.15255/CABEQ.2025.2429
49. *He, Y., Ren, S., Wang, X., Young, D., Mohamed-Said, M., Santos, B. A. F., Serenario, M. E. D., Singer, M.,* Temperature dependence of adsorption and effectiveness for a pyrimidinium-type corrosion inhibitor on mild steel, Corrosion **80** (2023) 177. doi: https://doi.org/10.5006/4346
50. *Alamiery, A. A.,* Comprehensive evaluation of 5-imino-1,2,4-dithiazolidine-3-thione as a corrosion inhibitor for mild steel in hydrochloric acid solution, Sci. Rep. **15** (2025) 10349. doi: https://doi.org/10.1038/s41598-025-95104-9
51. *Mansor, M., Baharin, N., Ghazali, S., Abidin, N., Zakaria, T., Dzulkifli, N.,* Corrosion inhibition pre-screening of nitrobenzaldehyde Meldrum's acid using response surface methodology (RSM) and Pearson correlation analysis, Pure Appl. Chem. **98** (2026) 537. doi: https://doi.org/10.1515/pac-2025-0556
52. *Lavanya, M., Hegde, B., Gaonkar, S. L., Gowri Shankar, M. C., Sinha, R. K., Kumari, P. P.,* Corrosion mitigation of 6061 aluminium alloy hybrid metal matrix composite using a green inhibitor: Experimental and theoretical investigations, Mater. Res. Express **11** (2024) 076510. doi: https://doi.org/10.1088/2053-1591/ad5e5f
53. *Hassan, R., Zaafarany, I., Gobouri, A., Takagi, H.,* A revisit to the corrosion inhibition of aluminum in aqueous alkaline solutions by water-soluble alginates and pectates as anionic polyelectrolyte inhibitors, Int. J. Corros. **1** (2013) 508596. doi: https://doi.org/10.1155/2013/508596
54. *Aljibori, H. S., Alamiery, A., Gaaz, T. S., Al-Azzawi, W. K.,* Exploring corrosion protection for mild steel in HCl solution: An experimental and theoretical analysis of an antipyrine derivative as an anticorrosion agent, Carbon Neutraliz. **3** (2024) 74. doi: https://doi.org/10.1002/cnl2.108
55. *Tang, H., Zhou, C., Li, J., Xiong, W., Chen, B., Peng, J., Pan, X., Guo, M., Xiao, Z., Dai, H., Luo, X., Liu, Y.,* In-depth insight into corrosion inhibition performance of sweet potato leaf extract as a green and efficient inhibitor for 6N01 Al alloy in the seawater: Experimental and theoretical perspectives, Langmuir **40** (2024) 9543. doi: https://doi.org/10.1021/acs.langmuir.4c00148

56. *Chung, I. M., Malathy, R., Kim, S. H., Kalaiselvi, K., Prabakaran, M., Gopiraman, M.,* Ecofriendly green inhibitor from *Hemerocallis fulva* against aluminum corrosion in sulphuric acid medium, J. Adhes. Sci. Technol. **34** (2020) 1483.
doi: https://doi.org/10.1080/01694243.2020.1712770
57. *Mobin, M., Zehra, S., Aslam, R.,* L-Phenylalanine methyl ester hydrochloride as a green corrosion inhibitor for mild steel in hydrochloric acid solution and the effect of surfactant additive, RSC Adv. **6** (2016) 5890.
doi: https://doi.org/10.1039/C5RA24630J
58. *Delijić, K., Boštjan, M.,* The influence of the chemical composition and type of alloy on corrosion performances of some medium strength Al-Mg-Si series of alloys, Metall. Mater. Eng. **20** (2014) 131.
doi: https://doi.org/10.5937/metmateng1402131D
59. *Khlopyk, O., Korniy, S., Zin, I., Holovchuk, M.,* Corrosion inhibition of aluminium alloy in NaCl solution by glycerol from biodiesel production, Chem. Eng. Commun. **211** (2024) 124.
doi: https://doi.org/10.1080/00986445.2023.2223126
60. *Zin, I. M., Korniy, S. A., Danyliak, M. O. M., Khlopyk, O. P., Holovchuk, M. Y.,* Anti-corrosion protection of aluminium alloy by zeolite doped with zinc, calcium and manganese cations, Int. J. Corros. Scale Inhib. **10** (2021) 1715.
doi: https://doi.org/10.17675/2305-6894-2021-10-4-22
61. *Guedes, L. A. L., Bacca, K. G., Lopes, N. F., da Costa, E. M.,* Tannin of acacia mearnsii as green corrosion inhibitor for AA7075-T6 alluminum alloy in acidic medium, Mater. Corros. **70** (2019) 1288.
doi: https://doi.org/10.1002/maco.201810667
62. *Mouats, N., Djellali, S., Ferkous, H., Sedik, A., Delimi, A., Boublia, A., Rachedi, K. O., Berredjem, M., Çukurovali, A., Alam, M., Ernsti, B., Benguerba, Y.,* Comprehensive investigation of the adsorption, corrosion inhibitory properties, and quantum calculations for 2-(2,4,5-trimethoxybenzylidene) hydrazine carbothioamide in mitigating corrosion of XC38 carbon steel under HCl environment, ACS Omega **9** (2024) 27945.
doi: https://doi.org/10.1021/acsomega.3c10240
63. *Xu, Y., Yi, G., Ma, H., Ju, D., Zhang, J., Hu, X., Zheng, C.,* Evaluation of ethylenediamine tetramethylene phosphonic sodium and zinc salts as a pipeline corrosion inhibitor via experimental and theoretical methods, Arab. J. Chem. **19** (2025) 6722025.
doi: https://doi.org/10.25259/AJC_672_2025
64. *Zhou, H., Chhin, D., Li, Y., Gallant, D., Morel, A., Mauzeroll, J.,* Quantitative interpretation of potentiodynamic polarization curves obtained at high scan rates in scanning electrochemical cell microscopy, Anal. Chem. **96** (2024) 15108.
doi: https://doi.org/10.1021/acs.analchem.4c01476
65. *Aballe, A., Bethencourt, M., Botana, F. J., Cano, M. J., Marcos, M.,* Inhibition of the corrosion process of alloy AA5083 (Al-Mg) in seawater by cerium cations. An EIS study, Mater. Corros. **52** (2001) 344.
doi: https://doi.org/10.1002/1521-4176(200105)52:5<344::AID-MACO344>3.0.CO;2-S
66. *Ali, A. I., Foaud, N.,* Inhibition of aluminum corrosion in hydrochloric acid solution using black mulberry extract, J. Mater. Environ. Sci. **3** (2012) 917.
67. *Pudjiwati, S., Sanusi, Y., Arwati, I. G. A.,* Use of hibiscus rosa-sinensisas a green corrosion inhibitor for valve materials in RO water, Adv. Mater **7** (2025), 88.
doi: https://doi.org/10.22441/ijimeam.v7i2.32806
68. *Khaled, R. H., Abdel-Gaber, A. M., Rahal, H. T., Awad, R.,* A potential green anti-scaling and corrosion inhibitor for mild steel in brine solution, Int. J. Electrochem. Sci. **15** (2020) 6790.
doi: https://doi.org/10.20964/2020.07.54
69. *Ait Aghzzaf, A., Veys-Renaux, D., Rocca, E.,* Pomegranate peels crude extract as a corrosion inhibitor of mild steel in HCl medium: Passivation and hydrophobic effect, Mater. Corros. **71** (2020) 148.
doi: https://doi.org/10.1002/maco.201911049